

Modulation of sensory information processing by a neuroglobin in *C. elegans*

Shigekazu Oda¹, Yu Toyoshima² and Mario de Bono¹

¹MRC Laboratory of Molecular Biology, Francis Crick Avenue, Cambridge CB2 0QH, UK;

²Department of Biochemistry and Biophysics, University of Tokyo, 2-11-16 Yayoi, Bunkyo-ku, Tokyo, Japan.

Summary

Sensory receptor neurons match their dynamic range to ecologically relevant stimulus intensities. How this tuning is achieved is poorly understood in most receptors. We show that in the *C. elegans* URX O₂ sensing neurons two putative molecular O₂ sensors, a neuroglobin and O₂-binding soluble guanylate cyclases, work antagonistically to sculpt a sharp sigmoidal O₂ response curve tuned to approach saturation when O₂ reaches 21%. *glb-5* imposes this sigmoidal function by inhibiting O₂-evoked Ca²⁺ responses in URX when O₂ levels fall. Without GLB-5, the URX response curve approaches saturation at 15% O₂. Behaviorally, GLB-5 signaling broadens the O₂ preference of *C. elegans* while maintaining strong avoidance of 21% O₂. Our computational aerotaxis model suggests that the relationship between GLB-5-modulated URX responses and reversal behavior is sufficient to broaden O₂-preference. Thus, a neuroglobin can shift neural information coding leading to a change in perception and altered behavior.

Introduction

Neuroglobins are members of the globin family of oxygen (O_2)-binding heme proteins expressed mainly in neurons¹. They have been described throughout metazoa, from cnidarians to man^{2,3}. Their physiological functions are poorly understood but they are proposed to protect neurons from hypoxia by metabolising reactive oxygen species (ROS), redox sensing or signalling, O_2 storage, control of apoptosis, and as negative regulators of Gi/o signalling⁴⁻⁹. In the nematode *Caenorhabditis elegans* the neuroglobin GLB-5 (*GLOBIN-5*) enables animals returned to normoxia after prolonged hypoxia exposure to accumulate rapidly where their bacterial food is thickest¹⁰. GLB-5, like vertebrate neuroglobins, has a hexa-coordinated heme iron, and rapidly oxidizes to the ferric state in normoxia¹¹. GLB-5 also plays a role in animals not exposed to hypoxia, modifying the function of specialized O_2 -sensing neurons^{11,12}. How GLB-5 changes the information coding properties of these neurons is unknown.

C. elegans avoids both high and low O_2 environments¹³. Avoiding high O_2 helps the animal escape surface exposure, and is mediated by sensory receptors that exhibit phasic-tonic responses, most importantly the URX neurons^{14,15}. URX, which express the GLB-5 neuroglobin^{11,12}, evoke both transient behavioral responses that are coupled to the rate of change of O_2 , dO_2/dt , and more persistent responses coupled to O_2 levels, $[O_2]$. The transient responses are reversals and turns that allow *C. elegans* to navigate O_2 gradients. The sustained responses involve a persistent switch to rapid movement as feeding animals seek to escape 21% O_2 . Besides *glb-5*, putative molecular O_2 sensors in URX include orthologs of the mammalian NO-binding soluble guanylate cyclases called GCY-35 and GCY-36^{13,16,17}. The heme – nitric oxide/oxygen (H-NOX) binding domain of GCY-35/GCY-36 is thought to stimulate cGMP production upon binding molecular O_2 .

The domesticated reference strain of *C. elegans*, N2, harbors a defective *glb-5* allele, but natural isolates encode a functional *glb-5(Haw)* allele^{11,12}. Here, we show that GLB-5(Haw) and the soluble guanylate cyclases work antagonistically to confer on URX a sharply sigmoidal O₂-stimulus–response curve tuned to saturate as O₂ levels approach 21%. The GLB-5 retuning of URX broadens the range of O₂ environments preferred by *C. elegans*. Using computer modelling we show that this altered preference can be explained by changes in how URX evokes reversals in response to O₂ stimuli.

Results

The GLB-5 allele in wild-caught strains broadens *C. elegans*' O₂ preference

To analyse how the functional *glb-5* allele found in natural *C. elegans* strains alters O₂ preference we compared the distribution of *glb-5(Haw)* and *glb-5(tm5440)* animals in a 0% – 21% O₂ gradient in the presence of food. The *glb-5(tm5440)* mutation deletes much of *glb-5* and is predicted to be a null allele. In all our experiments we used strains defective in the neuropeptide receptor *npr-1*, since besides harbouring a defective *glb-5* allele, the *C. elegans* lab strain, N2 (Bristol), has O₂-sensing defects due to a gain-of-function mutation in this receptor^{13,18}. *glb-5(tm5440)* animals accumulated in a narrow range of O₂ concentrations, between 7% and 10 % O₂ (Fig. 1a, b). By contrast, animals bearing the natural *glb-5(Haw)* allele distributed over a broader range of O₂ concentrations, between 17% and 5% O₂, but still avoided 21% O₂ and hypoxia (Fig. 1a, b). These behavioral data imply that *glb-5(Haw)* changes how O₂-sensing neurons decode O₂ gradients.

GLB-5 changes the dynamic range of the URX O₂ sensor

We used the GCaMP6s Ca²⁺ sensor to examine how *glb-5* function alters neural coding in the URX O₂-sensing neurons¹⁹. The dynamics of the Ca²⁺ responses evoked in URX by a 7% – 21% O₂ single step stimulus did not differ significantly between *glb-5(tm5440)* and *glb-5(Haw)* animals (Supplementary Fig. 1). However, the Ca²⁺ responses to a 7% – 19% O₂ exponential ramp stimulus differed markedly between these strains (Fig. 1c). In animals expressing *glb-5(Haw)*, Ca²⁺ in URX increased continuously as O₂ levels rose from 7% to 21%. By contrast, the Ca²⁺ responses of *glb-5(tm5440)* mutants appeared to saturate at ~14 % O₂. These differences suggest that the GLB-5 neuroglobin changes the dynamic range of URX, an observation we also made in PQR, another O₂ sensor that expresses GLB-5 (Fig. 1c). The effect of *glb-5* alleles on the URX Ca²⁺ response was similar whether we imaged animals in the presence (Fig. 1c) or absence of food (Supplementary Fig. 2). As expected, animals defective in both *glb-5* and the *gcy-35* soluble guanylate cyclase URX neurons did not respond to the O₂ stimulus (Fig. 1c).

To investigate further how the GLB-5 neuroglobin alters neural coding, we delivered different patterns of O₂ stimuli and imaged Ca²⁺ responses in URX. We focused on URX because these sensory neurons are sufficient for several O₂-coupled behaviors including aerotaxis (Supplementary Fig. 3) and aggregation^{20,21}. To plot the relationship between stimulus intensity and URX Ca²⁺ responses we sequentially increased the O₂ stimulus given to the same animal in 2% increments, returning to 7% O₂ between stimuli (Fig. 2a). In *glb-5(Haw)* animals URX showed a higher O₂-response threshold than *glb-5(tm5440)* mutants, as well as a steeply sigmoidal O₂ response curve whose half maximum was at much higher O₂ concentrations (Fig. 2a, b). Selectively expressing a *glb-5(Haw)* transgene in URX in *glb-5(tm5440)* mutants conferred a URX stimulus-

response profile that closely resembled that of *glb-5(Haw)* animals (Fig. 2a, b). Thus, GLB-5(Haw) cell-autonomously shifts the URX stimulus-response curve towards higher O₂ concentrations (Fig. 2b).

To extend these observations, we examined URX responses to a different set of stimuli in which we increased O₂ levels by 2% but varied the starting O₂ concentration and delivered only one stimulus per animal. Again, we observed that the *glb-5(Haw)* allele shifted the dynamic range of URX such that both tonic Ca²⁺ levels, and the change in Ca²⁺ normalized to the pre-stimulus Ca²⁺ level, $\Delta R/R_0$, a measure of response amplitude, gradually increased as O₂ approached 19% - 21% (Fig. 3a, b). By contrast, in *glb-5(tm5440)* mutants $\Delta R/R_0$ was at a maximum when animals experienced an 11→13 % O₂ stimulus (Fig. 3a, b). Expressing *glb-5(Haw)* cDNA selectively in URX in *glb-5(tm5440)* animals was sufficient to confer a *glb-5(Haw)*-like dose-response curve to this neuron (Fig. 3a, b).

Step stimulation is used widely to study the properties of sensory neurons, but in their natural environment *C. elegans* likely also encounter slowly varying O₂ levels, similar to those encountered by animals in the aerotaxis assay (Fig. 1a). We therefore measured URX Ca²⁺ responses evoked by a set of 2% O₂ exponential ramp stimuli. Our results showed a similar pattern to the one we observed for the corresponding step stimulus paradigm (Fig. 3c, d). In animals expressing the *glb-5(Haw)* allele, URX responses to ramp stimuli increased gradually as O₂ levels increased. By contrast, in *glb-5(tm5440)* mutants the URX response amplitudes, measured as $\Delta R/R_0$, showed a peak response to the 13→15 % O₂ stimulus and were otherwise similar across the different ramp stimuli we delivered (Fig. 3c,d). The response property changes conferred by GLB-5(Haw) are therefore robust to different O₂ stimulation patterns. Together, our

Ca^{2+} imaging experiments suggest that GLB-5(Haw) alters neural encoding of O_2 levels in URX, increasing the dynamic range of URX and shifting it to higher O_2 concentrations.

cGMP signalling in URX

In previous work we used the genetically-encoded cGMP sensor cGi500²² to visualize cGMP dynamics in the PQR O_2 sensing neuron¹⁷. We showed that a rise in O_2 stimulates a tonic GCY-35-dependent rise in cGMP, and that the Ca^{2+} influx resulting from gating of cGMP channels feeds back to limit O_2 -evoked rises in cGMP by stimulating cGMP hydrolysis¹⁷ (Supplementary Fig. 4a). We used cGi500 to examine if GLB-5(Haw) can modulate cGMP dynamics in URX. We could not detect O_2 -evoked cGMP responses in the cell body of URX neurons unless we disrupted *cng-1*, which encodes a cGMP-gated channel subunit required for O_2 -evoked Ca^{2+} responses in URX (Supplementary Fig. 4a, b). This suggests that URX and PQR have similar negative feedback control of cGMP accumulation. The cGMP responses evoked in URX by an exponential ramp O_2 stimulus was comparable in *glb-5(tm5440)*; *cng-1* and *glb-5(Haw)*; *cng-1* animals in our experimental conditions (Supplementary Fig. 4b,c). These results suggest that GLB-5(Haw) does not modulate URX neural coding by modulating cGMP levels. However, we cannot exclude the possibility that measuring cGMP in the cell body does not adequately report cGMP changes in the dendritic ending, where GLB-5, GCY-35/GCY-36 and the cGMP channels are localized.

Ectopic GLB-5 expression can alter the sensory properties of a CO_2 sensor

To explore the ability of GLB-5(Haw) neuroglobin to modify the properties of other neurons, we expressed it ectopically in the AFD sensory neurons. AFD neurons respond to both temperature²³ and CO_2 concentrations changes^{24,25} via mechanisms that involve

cGMP signalling. Animals expressing a *pAFD::glb-5(Haw)* transgene showed a larger transient decrease in Ca^{2+} upon exposure to increasing CO_2 concentrations than non-transgenic controls (Supplementary Fig. 5). These results suggest that *glb-5(Haw)* can actively alter neural encoding independently of the O_2 sensing mechanisms in URX. We next asked if GLB-5(Haw) expression can make AFD responsive to changes in O_2 , by imaging AFD Ca^{2+} while delivering O_2 stimuli. We found that GLB-5(Haw) conferred O_2 responsiveness to AFD, although responses were small (Supplementary Fig. 6). These results suggest that *glb-5(Haw)* neuroglobin can actively alter neural properties.

GLB-5 effects on URX behavioral outputs

How do the changes in URX information coding mediated by GLB-5(Haw) alter motor responses to O_2 stimuli? To address this question, we quantified behavioral responses to a range of O_2 stimuli, focusing on reversal and speed, which important features of O_2 -evoked behaviors^{20,21}. Avoidance of high O_2 is mediated principally by three sensory neurons, URX, PQR and AQR, each of which express the GCY-35/36 O_2 receptor and GLB-5^{10,12-14,16,20}. To focus on the behavioral consequences of URX output we studied *gcy-35(ok769)*; *glb-5(tm5440)* mutants that expressed *glb-5(Haw)* and / or *gcy-35* cDNA in URX but not AQR or PQR (see Methods). In these animals the relationship of URX output to reversals showed an unexpected Goldilocks effect (Fig. 4a, b). O_2 stimuli that evoked intermediate Ca^{2+} responses in URX in our imaging experiments evoked strong reversals (Fig. 3a, b and Fig. 4a, b). However, O_2 stimuli that evoked small or large Ca^{2+} responses in URX failed to evoke reversals (Fig. 3a, b and 4a, b). The effect of the *glb-5* genotype on reversals was consistent with its effect on the magnitude of the O_2 -evoked URX Ca^{2+} response (Fig. 3a, b and Fig 4a, b). These data suggest that URX associated circuits include a filter that prevents strong stimulation of

URX from inducing reversals. Consistent with this, a $13 \rightarrow 21\% \text{ O}_2$ step stimulus that evoked a large URX Ca^{2+} response did not evoke reversals (Supplementary Fig. 7). URX promoted faster movement only when O_2 levels rose above 17% O_2 (Fig. 4c, d). Together, our results suggest that information from URX is transmitted to both reversal and speed circuits, however, the transmission efficiency from URX to the reversal circuit is higher.

A computational model for aerotaxis

Using our detailed analyses of how URX responds to different O_2 stimuli we performed computational experiments to ask if the relationship between URX activity and reversal behavior could explain the altered aerotaxis preference of animals expressing *glb-5(Haw)*. To build a computational model for aerotaxis we used the Ca^{2+} imaging data in Fig 3a and the behavioral data in Figure 4c (see methods). In the model the position of a worm was represented as a single point, a command neuron randomly generates reversal, and a signal is transmitted from a URX model neuron to the command interneuron via an interneuron (differentiator) to promote reversal (Fig. 5a, see Methods). In the URX model, URX Ca^{2+} responses to O_2 stimuli were approximated by a Nonlinear-Linear-Nonlinear (NLN) model (Fig 5a). The parameters for the NLN model were estimated from imaging URX responses to 2% step O_2 stimuli in *glb-5(tm5440)* and *glb-5(Haw)* (Supplementary Fig. 8). A single model reproduced URX Ca^{2+} responses to a variety of O_2 changes. As a result of modeling the URX responses, we acquired two sets of parameters, one for *glb-5 (tm5440)* and the other one for *glb-5 (Haw)*. The parameters for steps downstream of URX were common for *glb-5 (tm5440)* and *glb-5 (Haw)* virtual animals.

Having set up our model we ran *in silico* aerotaxis experiments. These experiments

showed that worms in which the URX NLN model used parameters obtained for *glb-5(m5440)* preferred 7% – 10 % O₂ (Fig. 5b, c, Supplementary Fig. 9) whereas those using *glb-5(Haw)* parameters showed broader O₂ preference, with the majority of worms preferring 7% – 16 % O₂ (Fig. 5b, c, Supplementary Fig. 9). The predictions made by our computational model mirrored the results of aerotaxis experiments (Fig. 1a & Fig. 5b, c). To extend our model, we incorporated data on O₂-evoked changes in speed (Fig. 4c; Supplementary Fig. 10), in addition to O₂-evoked changes in reversals. We found this did not substantially change the performance of *glb-5(tm5440)* and *glb-5(Haw)* in virtual aerotaxis assays. Model worms that modulated both reversals and speed in response to O₂ changes distributed similarly to animals that modulated only reversal (Supplementary Fig. 11). By contrast, model worms in which changes in O₂ influenced only speed distributed almost evenly in a virtual aerotaxis chamber (Supplementary Fig. 11). Thus, in our model the relationship between URX response and reversal frequency is sufficient to account for the worm's O₂ preference in a shallow O₂ gradient.

Discussion

The neuroglobin GLB-5 changes how the URX O₂ sensing neurons encode O₂ concentration. URX sensory receptors enable *C. elegans* to avoid and escape 21% O₂. We find that URX neurons combine two putative molecular O₂ sensors, a soluble guanylate cyclase and a neuroglobin, to sculpt a sigmoidal O₂ tuning curve in which the neurons show little Ca²⁺ response to stimuli below 13% O₂, gradually increase their responsiveness above this O₂ concentration, and begin to saturate as O₂ approaches 21%. The neuroglobin GLB-5 imposes the sigmoidal function by inhibiting the O₂-evoked Ca²⁺ response in URX when O₂ levels fall below 21%. When GLB-5 is defective, the URX stimulus-response curve is shifted to lower O₂ levels and approaches saturation at

14% O₂. At a behavioral level, the effects of GLB-5 signaling is to broaden the O₂ environments preferred by *C. elegans* while maintaining strong avoidance of 21% O₂. If *glb-5* is defective, as in the N2 lab strain, animals prefer a narrow O₂ range, from 7% – 10%. Animals with functional *glb-5* signaling distribute more broadly, from 17% to 5% O₂. Some sensory responses exhibit steep sigmoidal tuning curves and it will be interesting to explore how frequently this is achieved by combining antagonistic molecular sensors. Studies of O₂ sensing in the glomus cells of the carotid bodies of mammals have implicated multiple O₂-sensing mechanisms that could act together to sculpt O₂ response features²⁸. Similarly, a range of CO₂/pH responsive molecules have been identified in mammals, although whether any of the numerous CO₂/pH-responsive cells use a combination of transducers is unclear²⁹.

Unexpectedly, we find that the relationship between URX Ca²⁺ response (a proxy of O₂ stimulus intensity) and behavioral output is nonlinear. Whereas intermediate stimulation of URX induces animals to reverse, strong stimulation is less effective. We have not investigated the neural mechanisms that underpin non-linear control of reversals by URX. However the neuroanatomical reconstructions reveal synapses from URX to both AVE interneurons that promote reversals, and to AVB interneurons that promote forward movement^{30,31} (<http://wormwiring.hpc.einstein.yu.edu/>) which could be differentially regulated according to URX stimulation.

Several computational model have been constructed to elucidate behavioral mechanisms underlying *C. elegans* taxis behavior^{26,27,32}. These models have been built using detailed observation of animals moving in gradients. A taxis model that incorporates experimentally-measured neural activities has not, however, been reported, but is required to understand how neural signals are processed and transformed to

behavior. We incorporated URX Ca^{2+} responses measured using GCaMP6s into a random walk model. These data can be extended into a more detailed model e. g. incorporating activities of interneurons and motor neurons, to probe the relationship between neural coding in sensory neurons, downstream neural circuits, and behavioral output.

How does the GLB-5 neuroglobin alter the Ca^{2+} responses of neurons at a molecular level? Like mammalian neuroglobin³³, GLB-5 rapidly oxidizes to a ferric form at 21% O_2 ¹¹, suggesting it could participate in ROS (reactive oxygen species) or redox signaling. In URX GLB-5 co-localizes with GCY-35/GCY-36 soluble guanylate cyclases at dendritic endings^{10,12}, and could potentially regulate the function of this other heme-binding protein. Our cGMP imaging did not support this hypothesis: we did not observe GLB-5-dependent differences in the O_2 -evoked responses of URX. However, the cGMP dynamics we measured in the URX cell body were very slow compared to the Ca^{2+} response, which implies that we are measuring a highly filtered response compared to the cGMP dynamics pertaining at the cGMP-gated channel. Although we do not exclude a role for GLB-5 in regulating soluble guanylate cyclases, our data suggest that GLB-5 can alter neural responses independently of these molecules. Expressing GLB-5 in the AFD sensory neurons altered their CO_2 -evoked Ca^{2+} responses; AFD neurons are not known to express soluble guanylate cyclases.

Neuroglobin has been suggested to protect neurons from hypoxia⁴. Our study shows that a neuroglobin can participate in neural information processing. The *C. elegans* genome encodes a variety of other neurally expressed globins that may similarly modify neural function³⁴. It would be interesting to investigate whether neuroglobin participates in information processing in vertebrate neural circuits.

Materials and methods

Strains

Strains were grown at 22-23 °C under standard conditions on Nematode Growth Medium (NGM) seeded with *Escherichia coli* OP50³⁵.

Neural imaging

Immobilized animals: Animals expressing GCaMP6s, cGi500, or YC3.60 were glued to agarose pads (2% in M9 buffer) using Dermabond tissue adhesive (Ethicon) with the nose and tail immersed in *E. coli* OP50. The glued worms were then covered with a PDMS (polydimethylsiloxane) miculofluidic chamber, as described previously¹⁴, and imaged using a 40x C-Apochromat lens on an inverted microscope (Axiovert; Zeiss) equipped with a Dual View emission splitter (Photometrics) and a Cascade II 512 EMCCD camera (Photometrics). The filters used were: GCaMP6s/mCherry: ex480/15 and 565/15 nm, di525/25 and 625/45 nm, em520/30 nm, em630/50 nm, di565 nm; YFP-CFP FRET: ex430/20 nm, di450 nm, em480/30 nm, em535/40 nm, di505 nm. Fluorescent images were captured at 1 fps with 2 x 2 or 1 x 1 binning using MetaMorph acquisition software (Molecular Devices). Data analysis used MATLAB (MathWorks) and Igor Pro (WaveMetrics). All time-lapse imaging data were denoised using binomial smoothing (Gaussian filter).

Delivery of gas stimuli: Humidified gas mixtures of defined composition were delivered using a PHD 2000 Infusion syringe pump (Harvard apparatus) at flow rates of 3.0, 2.0 and 1.0 ml/min. The syringes containing the gas were connected to PDMS chambers via polyethylene tubing and Teflon valves (AutoMate Scientific). A custom-built frame counter switched the valves at precise time points using TTL (transistor-transistor logic) pulses from the camera. To create the ramp stimulation, backlash air from the outlet of

the PDMS chamber was used. The O₂ stimuli in chambers were measured using an O₂ probe (Oxygen Sensor Spots PSt3, PreSens).

Behavioral assays

Aerotaxis assays were performed as described previously¹³ and animal positions noted 25 minutes into the assay. Briefly, rectangular PDMS chambers (dimensions of 33 x 15 x 0.2 mm) connected at either end to syringe pumps that delivered the indicated gas concentration were placed over 50 – 100 worms on a 9 cm NGM agar plate with food (*E. coli* OP50). The distribution of worms was recorded by counting animals in each of nine equal areas of the chamber.

To measure behavioral responses to step O₂-stimuli 5 adult hermaphrodites were placed on NGM plates seeded 36 – 40 h earlier with 20 μ l of *E. coli* OP50 grown in 2x TY medium. To create a behavioral arena with a defined atmosphere, we placed a PDMS chamber (1 x 1 x 0.2 cm) on top of the worms, with inlets connected to a PHD 2000 Infusion syringe pump (Harvard apparatus), and delivered humidified gas mixtures of defined composition at a flow rate of 3.0 ml/min. Movies were captured at 2fps using FlyCapture software (Point Grey) on a Point Grey Grasshopper camera (Point Grey) mounted on a Leica M165FC stereo microscope. Movies were analysed using custom-written MATLAB software to calculate instantaneous speed. Instantaneous speed data were denoised by binning over 6 seconds. Reversal frequency was counted manually. If the posterior and anterior tips of a worm's body moved backward until the worm stopped, this behavior was counted as 1 reversal; such events were often followed by turns.

Computational experiments and modelling

In the computational model, a worm was represented as a single point in a virtual field that represented an O₂ gradient in our experimental 18 mm (W) x 15 mm (L) aerotaxis chamber. O₂ levels in the virtual chamber varied from 7 % at W=0 mm to 21 % at W = 18

mm. The worm moved forward either at constant (~ 0.05 mm/sec) or at variable speed. For iterations when speed varied according to O_2 concentration at the animal's position we acquired parameters for speed by performing curve fitting with a Hill equation using the speed data shown in Fig. 4c (Supplementary Fig. 10b, c). The trend in an averaged time series was identified and removed based on gradient of the time series except frames from 241 to 300 (Supplementary Fig. 10a). If the worm reached the edge of the chamber, the direction of forward movement was reflected. The model worm has three modules that correspond to the sensory neuron (URX), an interneuron, and a command neuron (Fig. 5a). The information signal about O_2 level is transmitted from the sensory neuron to the command neuron through the interneuron. The activation of the command neuron leads a worm to start reversing. Reversals are expressed as a change in the direction of locomotion in the model. The locomotion direction after the reversal was randomly chosen from a uniform distribution ($0, 2\pi$) because experimentally measured reversals contain turning events. We assumed that the relationship between URX responses and reversal frequency was approximately linear in our model. This applies because animals in the virtual O_2 gradient, like those in a real-life aerotaxis assay, do not encounter large step O_2 stimuli.

The dynamics of the sensory circuit were represented by a Nonlinear-Linear-Nonlinear (NLN) model. The NLN model consisted of two nonlinear static filters and a linear temporal filter. O_2 stimulation was first converted by the input nonlinear filter, and processed by the temporal filter, then converted by the output nonlinear filter. The nonlinear filter $f(x)$ was expressed using a Hill equation,

$$f(x) = x^n / (x^n + x_0^n),$$

where x_0 and n were the parameters that defined the range and strength of the nonlinearity of the filter, respectively. For convenience, the input and output nonlinear filter are hereafter denoted as f_{in} and f_{out} , respectively. The linear temporal filter K has a 361 sample length ($t = 0, 1, \dots, 360$) and satisfies

$$y = UK,$$

where U and y are the input and output time courses of the temporal filter, respectively. This typical expression of temporal filter should be expanded because our dataset has multiple time courses (multi dose). If O_2 concentration is left as x , U can be written as

$$U = [U_1 \quad U_2 \quad \dots \quad U_{dmax}]^T,$$

$$U_d = f_{in} \left(\begin{bmatrix} x_d(0 - t_{max}) & x_d(1 - t_{max}) & \dots & x_d(0) \\ x_d(1 - t_{max}) & x_d(2 - t_{max}) & \dots & x_d(1) \\ \vdots & \vdots & \ddots & \vdots \\ x_d(0) & x_d(1) & \dots & x_d(t_{max}) \end{bmatrix} \right),$$

where $x_d(t)$ corresponds to the O_2 concentration at time t of d -th step stimulation and $x_d(t < 0)$ is replaced by $x_d(0)$. y can be expressed as

$$y = [y_1 \quad y_2 \quad \dots \quad y_{dmax}]^T,$$

$$y_d = [y_d(0) \quad y_d(1) \quad \dots \quad y_d(t_{max})]^T,$$

where $f_{out}(y_d(t))$ corresponds to the response of the sensory neuron at time t in response to d -th oxygen step stimulation. The linear temporal filter K can be obtained by evaluating

$$K = (U^T U)^{-1} U^T y.$$

For denoising, singular value decomposition was applied and the largest 100 components were used. In order to find the value of parameters of nonlinear filters, Nelder-Mead simplex optimization method was used and the sum of the square difference between $f_{out}(y_d(t))$ and corresponding experimental Ca^{2+} responses of URX

were minimized. Because this optimization was done separately for *glb-5(Haw)* and *glb-5(tm5440)*, we obtained two parameter sets for the NLN model.

Interneuron and command neuron were reasonably designed as described below. Because the worms show random reversals, the command neuron should be randomly activated. Furthermore, because the basal URX Ca^{2+} response (i.e. before stimulation of 2% change of oxygen) depends on the basal concentration of O_2 but basal reversal frequency does not, the model should contain a temporal differentiation functionality. Therefore, the activity of interneuron $g(t)$ was modelled as

$$g(t) = f_{out}(y_d(t)) - \sum_{\tau=1}^l f_{out}(y_d(t - \tau))/l ,$$

where l is a lag constant and was fixed as 11. The activity of command neuron is positive when

$$r < b * (1 + g(t) * c)$$

where b is the basal reversal frequency that is computed from experimental data, c is the coefficient of the effect of O_2 stimulation, and r is a uniformly distributed random number between 0 and 1. b and c were fixed to 0.0723 (reversal frequency per 1 second before a stimulation is given) and 3, respectively. Note that the parameters of interneuron and command neuron (l , b , and c) are independent of the *glb-5* genotype.

Strain list

AX5890, *glb-5(tm5440); npr-1(ad609); dbEx[gcy-32p::GCaMP6s, gcy-32p::mCherry, unc-122p::mCherry]*

AX5891, *glb-5(Haw); npr-1(ad609); dbEx[gcy-32p::GCaMP6s, gcy-32p::mCherry, unc-122p::mCherry]*

AX6075 *gcy-35(ok769); glb-5(tm5440); npr-1(ad609); dbEx[gcy-32p::GCaMP6s, gcy-32p::mCherry, unc-122p::mCherry]*

AX6088, *glb-5(tm5440); npr-1(ad609); dbEx[gcy-32p::GCaMP6s, gcy-32p::mCherry, unc-122p::mCherry]; dbEx[gcy-32p::glb-5 (Haw)::sl-2::mCherry, unc-122p::GFP]*

AX1891, *glb-5(Haw); npr-1(ad609)*

AX5935, *gcy-35(ok769); glb-5(tm5440); npr-1(ad609)*

AX5936, *gcy-35(ok769); glb-5(tm5440); npr-1(ad609); dbEx[flp-8p::gcy-35::gfp, unc-122p::gfp]*

AX6124, *gcy-35(ok769); glb-5(tm5440); npr-1(ad609); dbEx[flp-8p::gcy-35::gfp, unc-122p::gfp], dbEx[flp-8p::glb-5::sl-2::mCherry, lin-44p::GFP]*

AX1908, *glb-5(Haw); npr-1(ad609) lin-15(n765ts); dbEx[gcy-32p::YC3.60, lin-15(+)]*

AX5850, *glb-5(tm5440); npr-1(ad609) lin-15(n765ts); dbEx[gcy-32p::YC3.60, lin-15(+)]*

AX3535, *glb-5(tm5440); npr-1(ad609)*

AX5779, *dbEx[gcy-8p::YC3.60, odr-1p::mCherry]; dbEx[gcy-8p::glb-5 (Haw)]*

AX2047, *dbEx[gcy-8p::YC3.60, odr-1p::mCherry]*

AX2417, *glb-5(Haw); cng-1(db111); npr-1(ad609); dbEx[gcy-37p::cGi500]*

AX6024, *glb-5(tm5440); cng-1(db111); npr-1(ad609); dbEx[gcy-37p::cGi500]*

AX2084, *glb-5(Haw); npr-1(ad609); dbEx[gcy-37p::cGi500]*

AX6012, *glb-5(tm5440); npr-1(ad609); dbEx[gcy-37p::cGi500]*

Acknowledgements

We thank the National Bioresource Project for strains, W.R. Schafer and Y. Iino for plasmids, and I. Beets, L. Fenk, T. Tomida and S. Laughlin for comments on the manuscript. This work was supported by the Medical Research Council (MC_U105178786), European Research Council (269058 ACMO), Uehara Memorial Foundation (S.O.), Grants-in-Aid for Young Scientists (B) (26830006) (Y.T.) and for

Grant-in-Aid for Scientific Research on Innovative Areas (16H01418) from the Ministry of Education, Culture, Sports, Science and Technology of Japan (Y.T.).

References

1. Burmester, T. & Hankeln, T. Function and evolution of vertebrate globins. *Acta Physiol (Oxf)* **211**, 501-514 (2014).
2. Burmester, T., Weich, B., Reinhardt, S. & Hankeln, T. A vertebrate globin expressed in the brain. *Nature* **407**, 520-523 (2000).
3. Lechauve, C. et al. Neuroglobins, pivotal proteins associated with emerging neural systems and precursors of metazoan globin diversity. *J Biol Chem* **288**, 6957-6967 (2013).
4. Burmester, T. & Hankeln, T. What is the function of neuroglobin? *J Exp Biol* **212**, 1423-1428 (2009).
5. Li, W. et al. The activity of recombinant human neuroglobin as an antioxidant and free radical scavenger. *Proteins* **79**, 115-125 (2011).
6. Fago, A., Mathews, A. J. & Brittain, T. A role for neuroglobin: resetting the trigger level for apoptosis in neuronal and retinal cells. *IUBMB Life* **60**, 398-401 (2008).
7. Tiso, M. et al. Human neuroglobin functions as a redox-regulated nitrite reductase. *J Biol Chem* **286**, 18277-18289 (2011).
8. Wakasugi, K., Nakano, T. & Morishima, I. Oxidized human neuroglobin acts as a heterotrimeric Galph protein guanine nucleotide dissociation inhibitor. *J Biol Chem* **278**, 36505-36512 (2003).
9. Ascenzi, P., Gustincich, S. & Marino, M. Mammalian nerve globins in search of functions. *IUBMB Life* **66**, 268-276 (2014).
10. Gross, E. et al. GLOBIN-5-dependent O₂ responses are regulated by PDL-1/PrBP

that targets prenylated soluble guanylate cyclases to dendritic endings. *J Neurosci* **34**, 16726-16738 (2014).

11. Persson, A. et al. Natural variation in a neural globin tunes oxygen sensing in wild *Caenorhabditis elegans*. *Nature* **458**, 1030-1033 (2009).
12. McGrath, P. T. et al. Quantitative mapping of a digenic behavioral trait implicates globin variation in *C. elegans* sensory behaviors. *Neuron* **61**, 692-699 (2009).
13. Gray, J. M. et al. Oxygen sensation and social feeding mediated by a *C. elegans* guanylate cyclase homologue. *Nature* **430**, 317-322 (2004).
14. Busch, K. E. et al. Tonic signaling from O(2) sensors sets neural circuit activity and behavioral state. *Nat Neurosci* **15**, 581-591 (2012).
15. Zimmer, M. et al. Neurons detect increases and decreases in oxygen levels using distinct guanylate cyclases. *Neuron* **61**, 865-879 (2009).
16. Cheung, B. H., Arellano-Carbalal, F., Rybicki, I. & De Bono, M. Soluble Guanylate Cyclases Act in Neurons Exposed to the Body Fluid to Promote *C. elegans* Aggregation Behavior. *Curr. Biol.* **14**, 1105-1111 (2004).
17. Couto, A., Oda, S., Nikolaev, V. O., Soltesz, Z. & de Bono, M. In vivo genetic dissection of O2-evoked cGMP dynamics in a *Caenorhabditis elegans* gas sensor. *Proc Natl Acad Sci U S A* **110**, E3301-10 (2013).
18. de Bono, M. & Bargmann, C. I. Natural variation in a neuropeptide Y receptor homolog modifies social behavior and food response in *C. elegans*. *Cell* **94**, 679-689 (1998).
19. Chen, T. W. et al. Ultrasensitive fluorescent proteins for imaging neuronal activity. *Nature* **499**, 295-300 (2013).
20. Cheung, B. H., Cohen, M., Rogers, C., Albayram, O. & de Bono, M. Experience-dependent modulation of *C. elegans* behavior by ambient oxygen. *Curr Biol* **15**,

905-917 (2005).

21. Rogers, C., Persson, A., Cheung, B. & de Bono, M. Behavioral motifs and neural pathways coordinating O₂ responses and aggregation in *C. elegans*. *Curr Biol* **16**, 649-659 (2006).
22. Russwurm, M. et al. Design of fluorescence resonance energy transfer (FRET)-based cGMP indicators: a systematic approach. *Biochem J* **407**, 69-77 (2007).
23. Kimura, K. D., Miyawaki, A., Matsumoto, K. & Mori, I. The *C. elegans* thermosensory neuron AFD responds to warming. *Curr Biol* **14**, 1291-1295 (2004).
24. Bretscher, A. J. et al. Temperature, Oxygen, and Salt-Sensing Neurons in *C. elegans* Are Carbon Dioxide Sensors that Control Avoidance Behavior. *Neuron* **69**, 1099-1113 (2011).
25. Kodama-Namba, E. et al. Cross-modulation of homeostatic responses to temperature, oxygen and carbon dioxide in *C. elegans*. *PLoS Genet* **9**, e1004011 (2013).
26. Pierce-Shimomura, J. T., Morse, T. M. & Lockery, S. R. The fundamental role of pirouettes in *Caenorhabditis elegans* chemotaxis. *J Neurosci* **19**, 9557-9569 (1999).
27. Iino, Y. & Yoshida, K. Parallel use of two behavioral mechanisms for chemotaxis in *Caenorhabditis elegans*. *J Neurosci* **29**, 5370-5380 (2009).
28. Lopez-Barneo, J. et al. Oxygen sensing by the carotid body: mechanisms and role in adaptation to hypoxia. *Am J Physiol Cell Physiol* **310**, C629-42 (2016).
29. Huckstepp, R. T. & Dale, N. Redefining the components of central CO₂ chemosensitivity--towards a better understanding of mechanism. *J Physiol* **589**, 5561-5579 (2011).
30. White, J. G., Southgate, E., Thomson, J. N. & Brenner, S. The structure of the

nervous system of the nematode *Caenorhabditis elegans*. *Philosophical Transactions of the Royal Society of London B*, 1-340 (1986).

31. Chalfie, M. et al. The neural circuit for touch sensitivity in *Caenorhabditis elegans*. *J Neurosci* **5**, 956-964 (1985).
32. Roberts, W. M. et al. A stochastic neuronal model predicts random search behaviors at multiple spatial scales in *C. elegans*. *Elife* **5**, (2016).
33. Dewilde, S. et al. Biochemical characterization and ligand binding properties of neuroglobin, a novel member of the globin family. *J Biol Chem* **276**, 38949-38955 (2001).
34. Tilleman, L. et al. Globins in *Caenorhabditis elegans*. *IUBMB Life* **63**, 166-174 (2011).
35. Sulston, J. & Hodgkin, J. in *The nematode Caenorhabditis elegans* (ed Wood, W. B.) 587-606 (CSHL Press, Cold Spring Harbor, 1988).

Figure Legends

Figure 1 The GLB-5 neuroglobin broadens *C. elegans*' O₂ preference

(a) Aerotaxis behavior. Distribution of animals in a 0 – 21% O₂ gradient. N = 6. Plots show mean +/- s.e.m. **(b)** The *glb-5(Haw)* allele broadens *C. elegans*' O₂ preference. High O₂ avoidance index = (fraction of animals in 7%–14% O₂) – (fraction of animals in 14–21% O₂) / (fraction of animals in 7– 21% O₂). O₂ preference (7–10 % O₂) = (fraction of animals in 7%–10% O₂) / (fraction of animals in 7%– 21% O₂). **p < 0.01, Mann-Whitney U-test. Data are from **a**. **(c)** Mean Ca²⁺ responses of URX and PQR neurons to the indicated O₂ ramp stimulus. N = 10–12. Shading represents s.e.m. Ca²⁺ sensors were GCaMP6s co-expressed with mCherry (URX) and YC3.60 (PQR). The URX plot also shows the responses of *gcy-35*; *glb-5(tm5440)* mutants; GCY-35 is required for

measurable O₂-evoked Ca²⁺ responses. The O₂ ramp stimulus (top) shows the mean of 4 measurements +/- s.e.m.

Figure 2 GLB-5 changes the stimulus-response curve of O₂-evoked Ca²⁺ responses in URX

(a) Ca²⁺ responses evoked in URX by a graded series of O₂ steps that start from a 7% O₂ baseline (N = 10). Data show mean +/- s.e.m. Responses are normalised to the GCaMP6s/mCherry ratio averaged over the 10 secs prior to delivery of the stimulus train.

(b) Maximum amplitude of the responses from **(a)** plotted against O₂ stimulus intensity. Bars represent s.e.m. *, p < 0.05; ** p < 0.01; *glb-5(Haw)* vs *glb-5(tm5440)*. ++, p < 0.01; *glb-5(tm5440)* *URXp::glb-5(Haw)* vs *glb-5(tm5440)*. ANOVA with Dunnett's post hoc test.

Figure 3 Coding of step and ramp O₂ stimuli by URX

(a) Averaged traces of the Ca²⁺ response of URX to different 2% O₂ step stimuli in *glb-5(Haw)*, *glb-5(tm5440)*, and *glb-5(tm5440); pgcy-32::glb-5(Haw)* animals. N = 10-13. **b**, Maximum amplitudes of the responses shown in **a** plotted against stimulus intensity. Data show mean +/- s.e.m.. **(c)** Averaged traces of the Ca²⁺ response of URX to different 2% O₂ ramp stimuli in *glb-5(Haw)* and *glb-5(tm5440)* animals. N = 11 – 13. **d**, Maximum amplitude of the responses shown in **c** plotted against stimulus intensity. Data show mean and s.e.m. The O₂ plots of a step and a ramp stimulus at top of **a** and **c** show the mean of 9 (**a**) and 10 (**c**) measurements +/- s.e.m. *, p < 0.05; ** p < 0.01; *glb-5(Haw)* vs *glb-5(tm5440)*. +, p < 0.05; ++, p < 0.01; *glb-5(tm5440)* *URXp::glb-5(Haw)* vs *glb-5(tm5440)*. ANOVA with Dunnett's post hoc test (b). Mann-Whitney U test (d).

Figure 4 The relationship between O₂ stimulus intensity and URX-dependent behavioral outputs

(a) Frequency of reversal behavior evoked by O₂ step stimuli in animals of the genotypes indicated. Reversal frequencies were quantified every minute. N = 15-30 animals. Bars represent s.e.m. (b) Reversal frequency evoked by step O₂ stimuli averaged over 4 minutes after the stimulus. Data represent mean +/- s.e.m. (c, d) Instantaneous speed in response to step O₂ stimuli indicated. N = 30-60 animals. Plots show mean +/- s.e.m. (d) Mean speed +/- s.e.m calculated for a 4 minute interval beginning 30 seconds after the step stimulus. The behavior of *gcy-35(ok769); glb-5(tm5440)* animals was used as a negative control, and is shown as black traces or grey bars. *P < 0.05, **P < 0.01, ANOVA with Dunnett's post hoc test. NS, not significant.

Figure 5 A computational model that links O₂-evoked Ca²⁺ responses in URX to behavioral output

(a) Schematic of the computational model. (b) Heat map representing the location of 10000 fictive *glb-5(tm5440)* or *glb-5(Haw)* animals in a 7% to 21% O₂ gradient. Locations are plotted every second. (c) Histograms of the existence frequency of *glb-5(tm5440)* and *glb-5(Haw)* in a 7% to 21% O₂ gradient during the last 100 seconds of the computational experiments shown in b. The fictive URX responses and reversal frequency of these model worms during aerotaxis are shown in Supplementary Fig. 9.

Supplementary Figure Legends

Supplementary Figure 1 The URX Ca²⁺ response to strong stimulation

a. Mean URX Ca^{2+} responses to a 7% to 21% O_2 stimulus in *glb-5(Haw)* (red trace) and *glb-5(tm5440)* (blue trace) animals. N = 8. Shading represents s.e.m. **b.** Peak $\Delta R/R_0$ +/- s.e.m. evoked by the O_2 stimulus in **a**. NS, not significant (Mann-Whitney U-test).

Supplementary Figure 2 URX Ca^{2+} responses to an exponential ramp O_2 stimulus in the absence of food

Ca^{2+} responses in URX evoked by an exponential ramp O_2 stimulus in *glb-5(tm5440)* (blue trace) and *glb-5(Haw)* (red trace) animals imaged in the absence of food. N = 10. Shading represents s.e.m. The Ca^{2+} sensor was GCaMP6s (co-expressed with mCherry). The O_2 stimulus used is shown above the traces, plotted as the mean O_2 concentration +/- s.e.m. N = 4.

Supplementary Figure 3 Expressing *glb-5(Haw)* in URX is sufficient to change *C. elegans*' O_2 preference

Aerotaxis of *C. elegans* expressing *gcy-35* or *gcy-35* and *glb-5(Haw)* selectively in URX. *glb-5(tm5440)* is a positive control and the same *dbExpflp-8::gcy-35* transgenic line was used with or without the *pURX::glb-5(Haw)* transgene. N = 5-6. Data plotted are Mean +/- s.e.m.

Supplementary Figure 4 O_2 -evoked cGMP responses in URX

(a) Model of sensory transduction of O_2 stimuli in URX. **(b)** cGMP responses evoked in URX by an exponential O_2 ramp stimulus. Data show Mean +/- s.e.m. Top: traces from *glb-5(tm5440)* (blue) and *glb-5(Haw)* (red) animals. Bottom: traces from *cng-1(db111)*; *glb-5(tm5440)* (blue) and *cng-1(db111)*; *glb-5(Haw)* (red) animals. N = 10-11. The O_2

stimulus used is plotted on top of the cGMP traces. Data show Mean O₂ +/- s.e.m. N = 4.

(c) Average responses compared at time points indicated by the black bar in **b** (bottom). NS, not significant (Mann-Whitney U-test).

Supplementary Figure 5 Ectopic expression of GLB-5(Haw) in AFD alters CO₂-evoked Ca²⁺ responses in this neuron

(a) Mean Ca²⁺ responses evoked by a series of CO₂ stimuli in AFD neurons in animals with or without ectopic expression of *glb-5(Haw)* in AFD. N = 10-11. The sensor is YC3.60. The background O₂ concentration in these experiments was 11 % O₂. Traces were normalized using the average YFP/CFP ratio for the 10 secs immediately before delivery of each CO₂ step in the train. (b, c) Minimum (b) or maximum (c) values of AFD Ca²⁺ responses upon CO₂ exposure or removal plotted against stimulation intensity. Values are normalized using the average YFP/CFP ratio for 10 the sec immediately prior to each CO₂ upstep (b) or downstep (c). Error bars represent s.e.m. *P < 0.05, Mann-Whitney U-test.

Supplementary Figure 6 GLB-5(Haw) confers O₂ responsiveness to the AFD sensory neuron

(a,b) Ca²⁺ responses evoked by indicated O₂ stimuli in wild type AFD or AFD that ectopically express *glb-5(Haw)*. N = 9-13. The sensor is YC3.60. (c, d) The maximum Ca²⁺ response over a 30 second interval at 21% O₂ from a, b. * p < 0.05; ** p < 0.01, Mann-Whitney U-test.

Supplementary Figure 7 Strong stimulation of URX does not induce reversals

(a) Mean URX Ca^{2+} response evoked by a $13 \rightarrow 21\%$ step O_2 stimulus in genotypes indicated. Shading represents s.e.m. **(b)** Reversal frequencies of *C. elegans* in response to a $13 \rightarrow 21\%$ step O_2 stimulus. Reversal frequency was quantified every one minute ($N = 14\text{--}20$ animals). Bars represent s.e.m.

Supplementary Figure 8 NLN model: reconstruction of URX responses

Reconstruction by the NLN model of Ca^{2+} responses evoked in URX by 2% O_2 step stimuli in *glb-5(Haw)* and *glb-5(tm5440)* animals. Solid and dashed lines indicate reconstructed data and experimental data, respectively. The experimental data used for comparison are taken from Fig. 3a, b.

Supplementary Figure 9 URX responses and reversal frequency of model worms in Fig. 5

(a,b) Histograms of fictive URX responses of *glb-5(tm5440)* **(a)** and *glb-5(Haw)* **(b)** model worms over the 1800 sec of the *in silico* experiment shown in Fig. 4. **c**, Simulated tracks of three worms navigating the O_2 gradient in our computer simulations. Shown are 1801 steps. The X and Y axis are the dimensions of the fictive aerotaxis chambers. Colors code local O_2 concentration. **d**, Reversal frequency at each O_2 concentration of the model worms during the 1800 sec. Red and blue traces indicate fictive *glb-5(Haw)* and *glb-5(tm5440)* animals respectively.

Supplementary Figure 10 Data processing of speed data for computational experiments

(a) De-trending speed data. To incorporate experimental speed data into our model, we identified and removed a slow downward trend in an averaged time series of the speed of animals responding to O_2 cues. The raw experimental speed data (from Fig. 4c) are shown on the left, with the dashed lines showing the fitted lines used for detrending. The de-trended data is on the right. . **(b, c)** De-trended average speed before (triangle) or after (circle) we delivered the O_2 stimuli described in Fig. 3. By performing curve fitting on this data we acquired parameters for the Hill equation used in the computational experiments,

Supplementary Figure 11 Modeling how O_2 -evoked changes in speed alters O_2 -preference in aerotaxis assays

Instantaneous location of 10,000 fictive *glb-5(tm5440)* and *glb-5(Haw)* animals in different aerotaxis models, plotted at 1 sec intervals and represented by heat maps. Top: fictive animals have constant speed but show O_2 -evoked reversals according to our model for URX output. Middle: Fictive animals show O_2 -evoked changes in speed according to our model for URX output but not in reversals. Bottom: fictive animals show O_2 -evoked changes in both reversals and speed. Histograms show the existence frequency of model worms during the last 100 seconds of the computational experiments.

Fig. 1

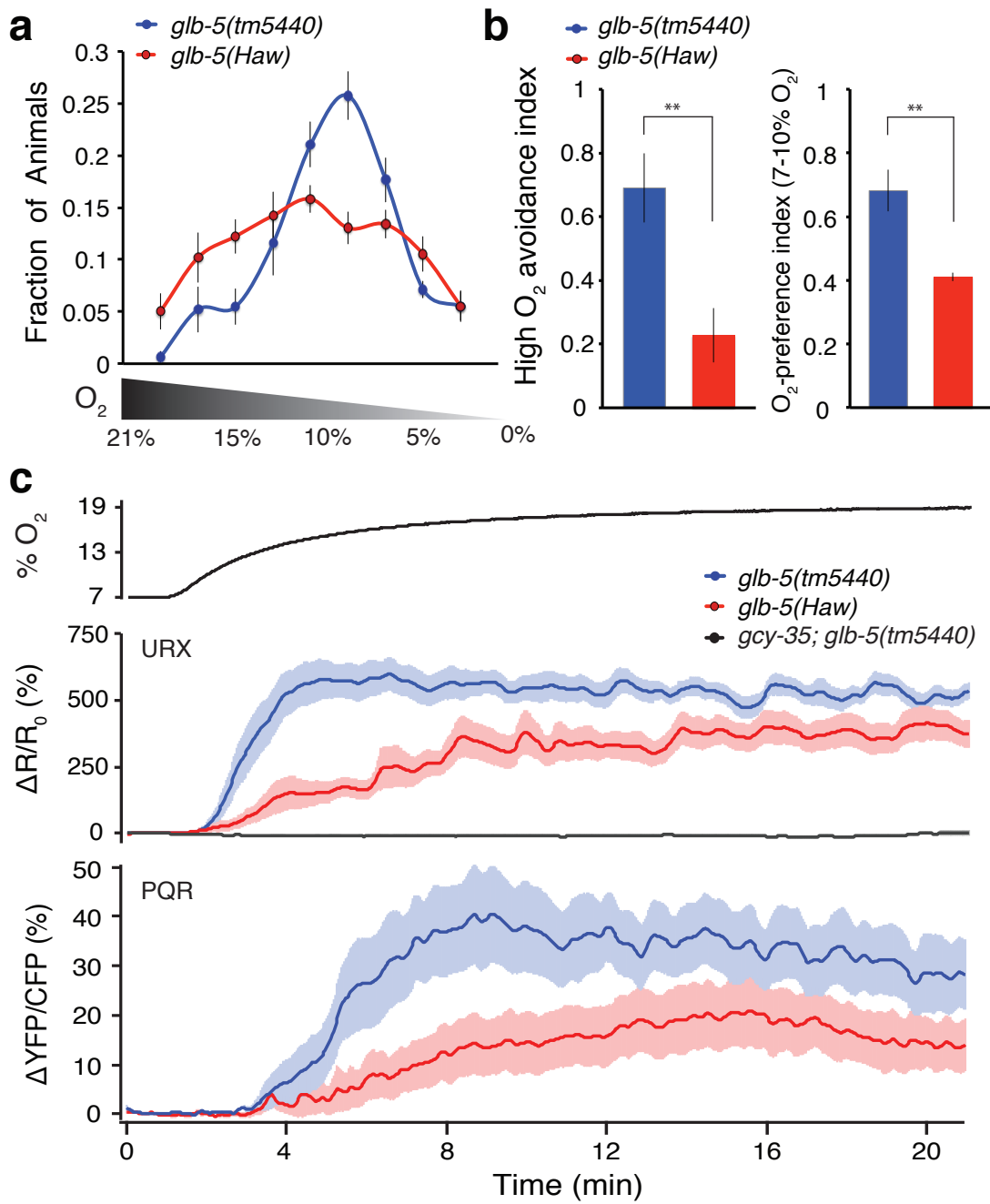


Fig. 2

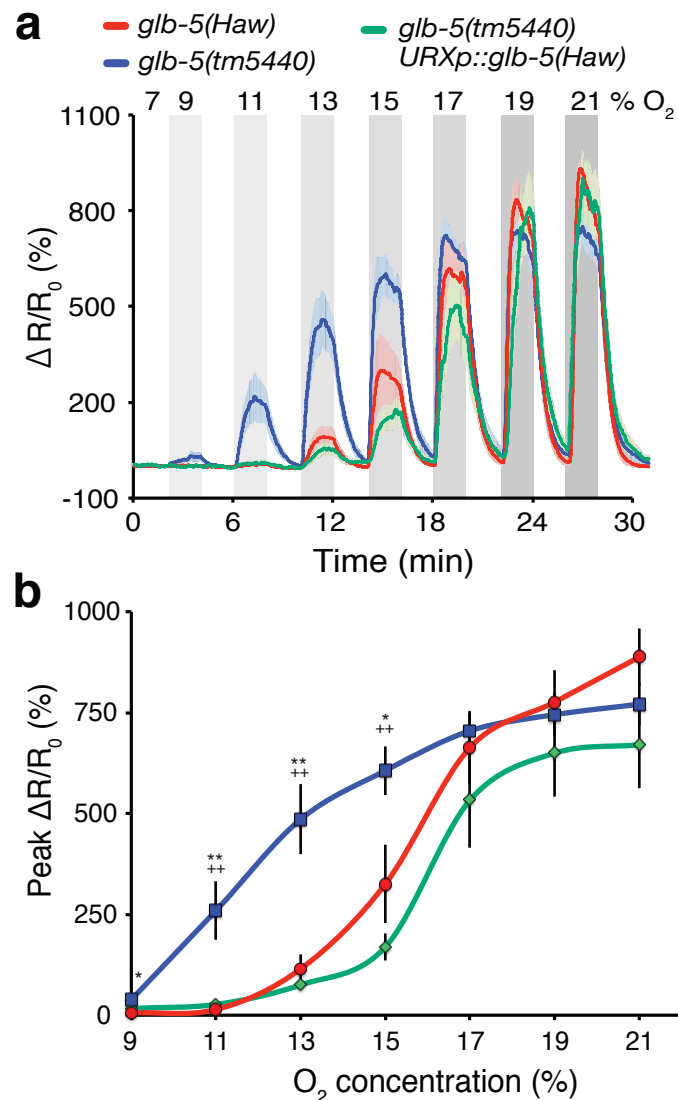
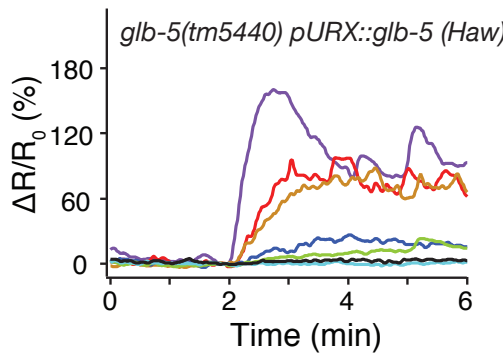
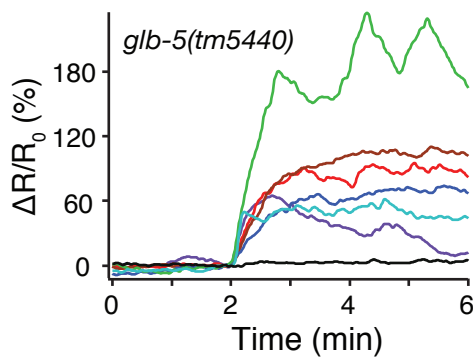
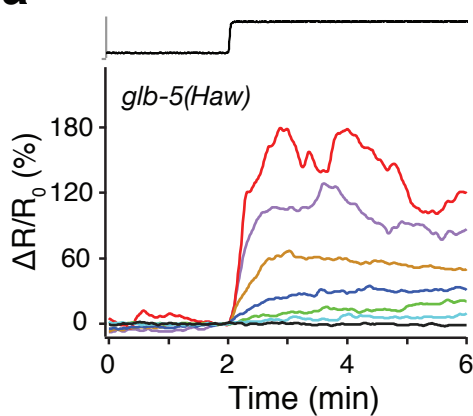


Fig. 3

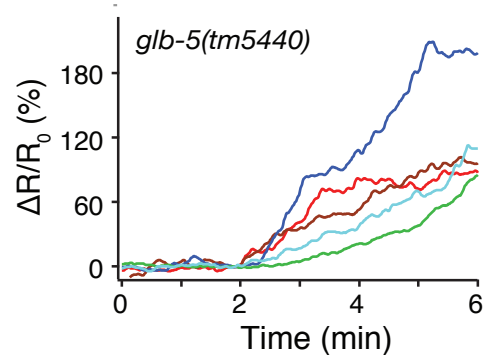
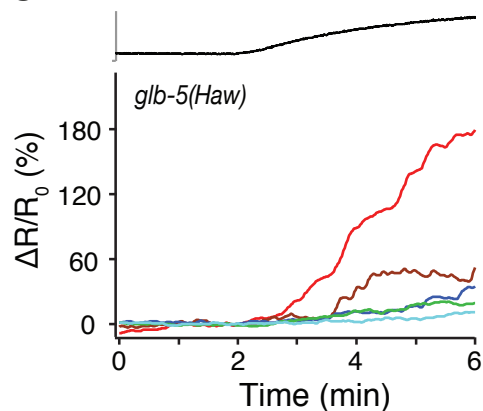
a



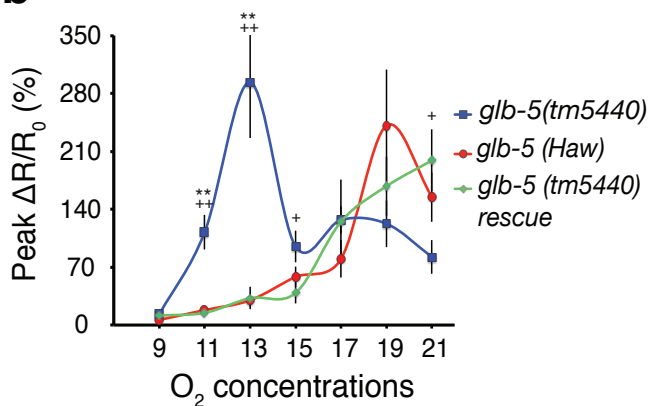
Stimulus (% O₂)

- 19 -> 21
- 17 -> 19
- 15 -> 17
- 13 -> 15
- 11 -> 13
- 9 -> 11
- 7 -> 9

c



b



d

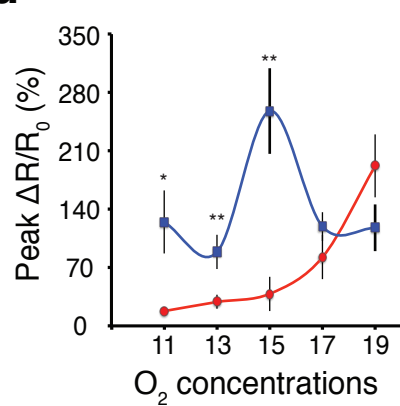


Fig. 4

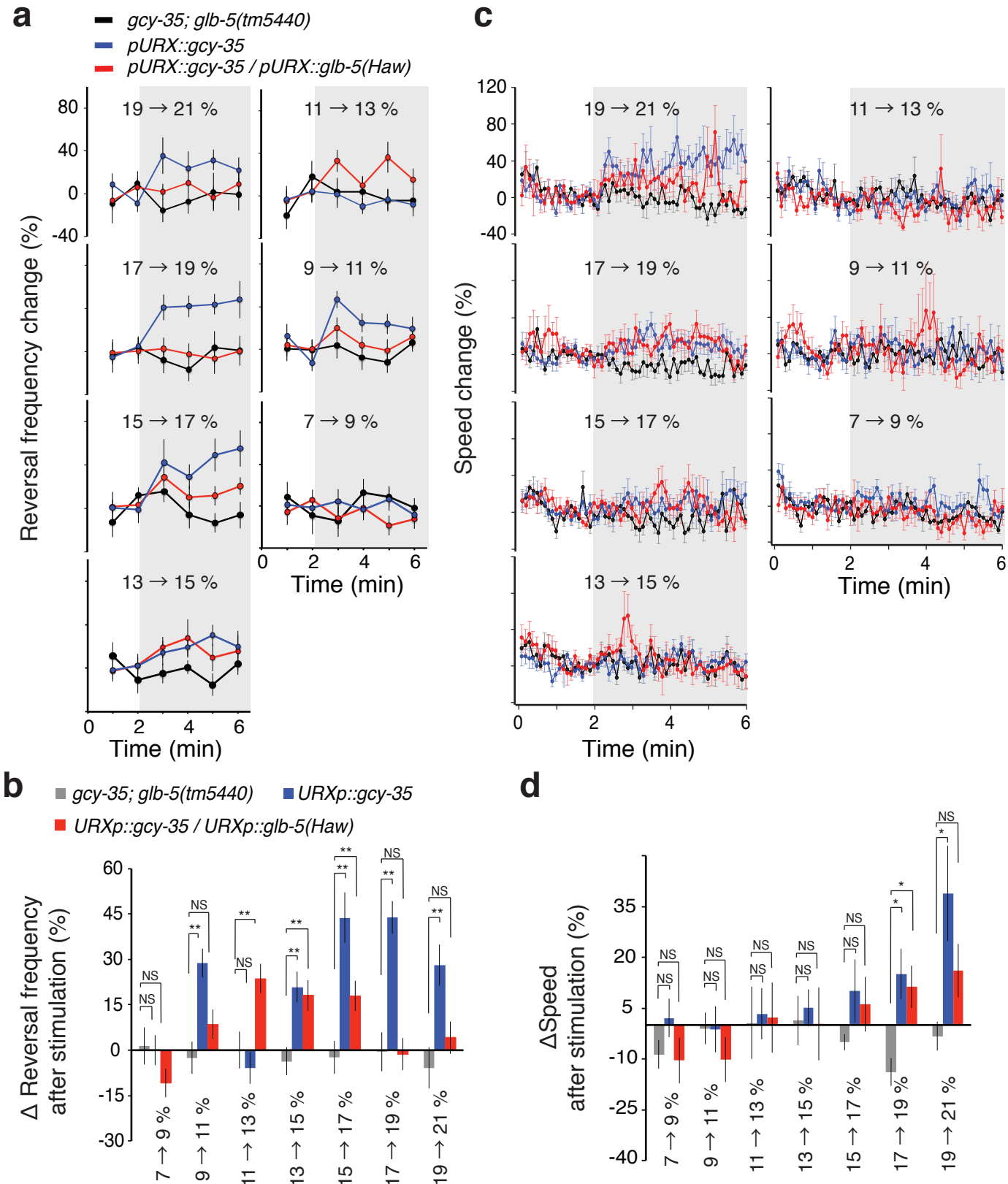
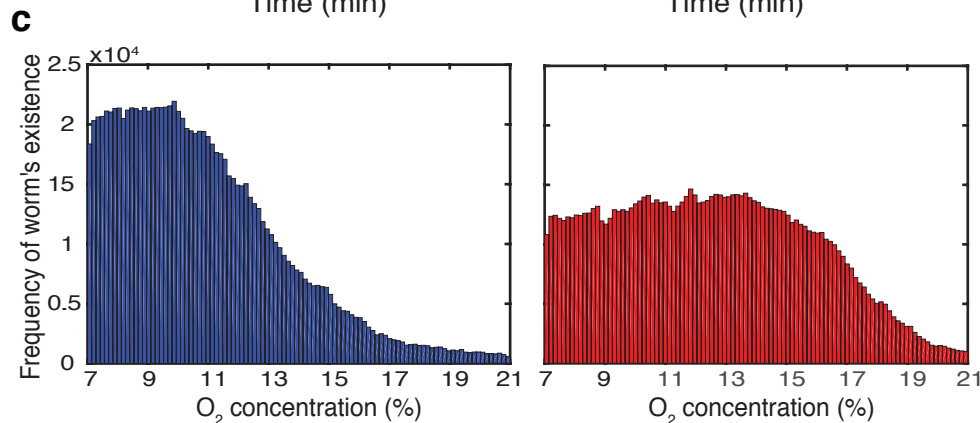
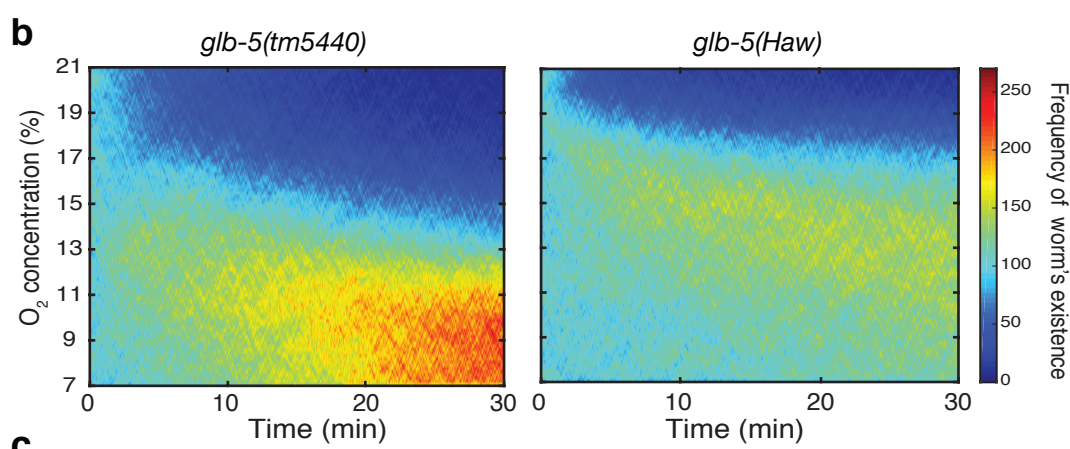
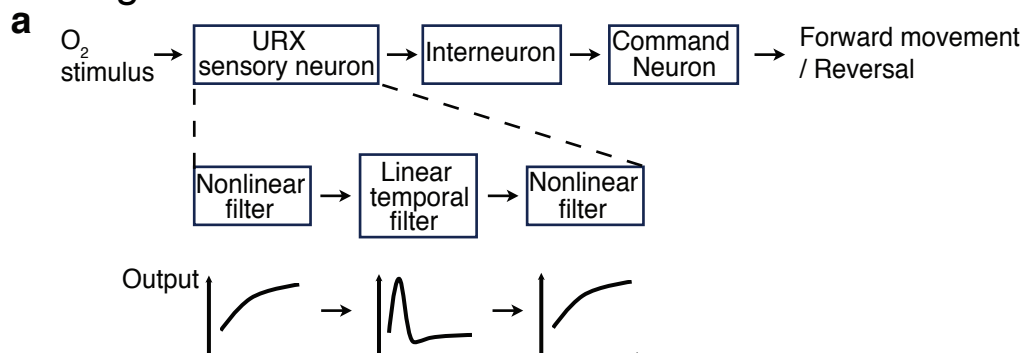
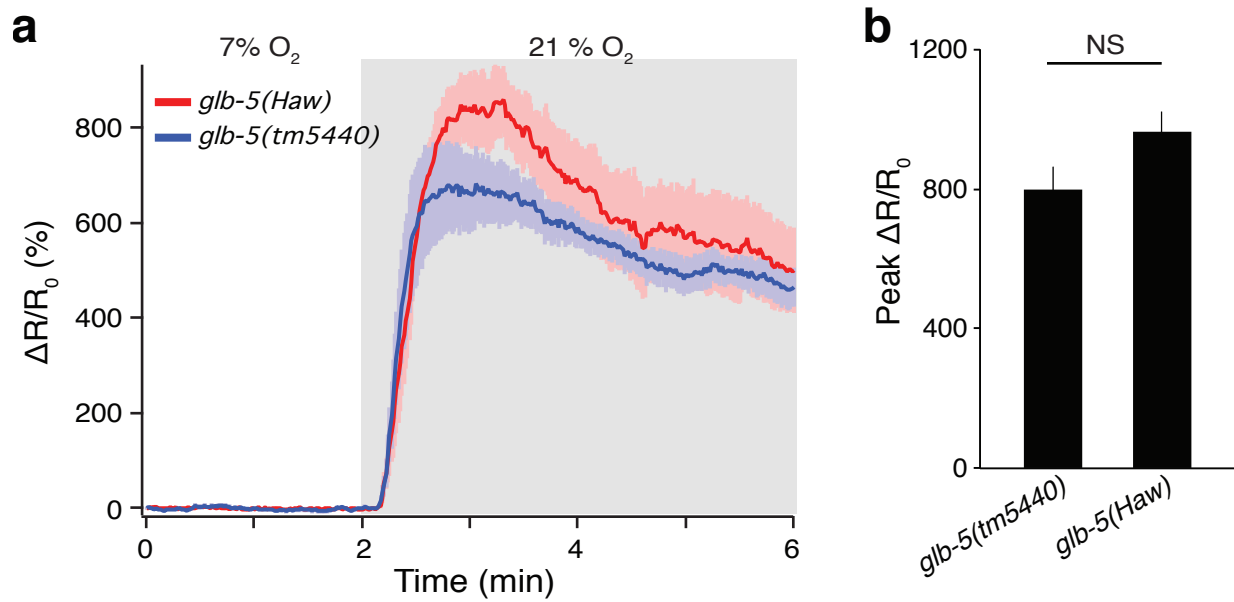


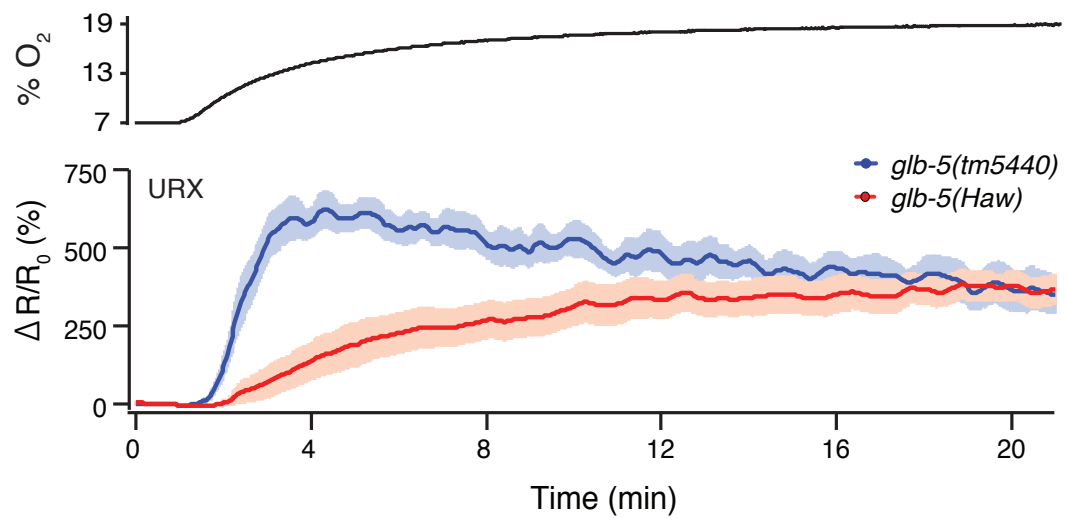
Fig. 5



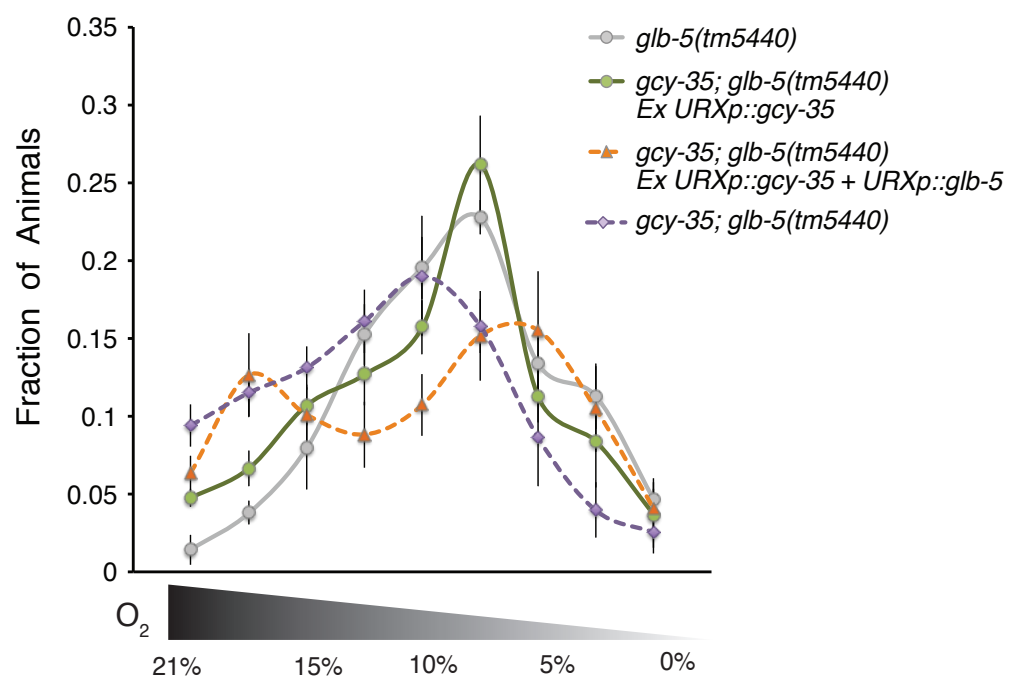
SFig 1



SFig 2

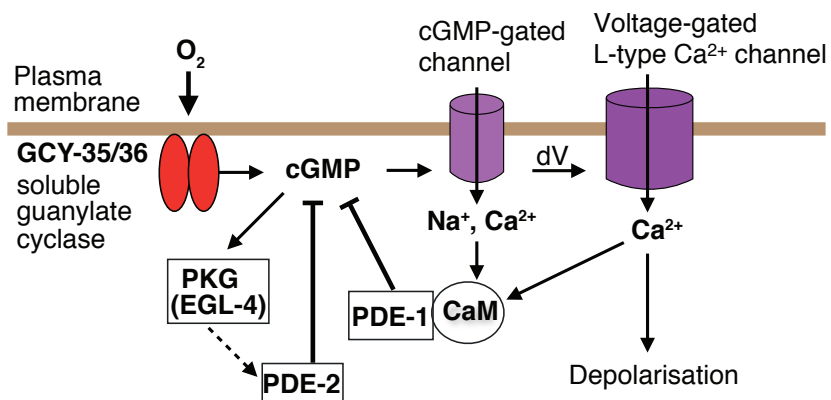


Supp Fig 3

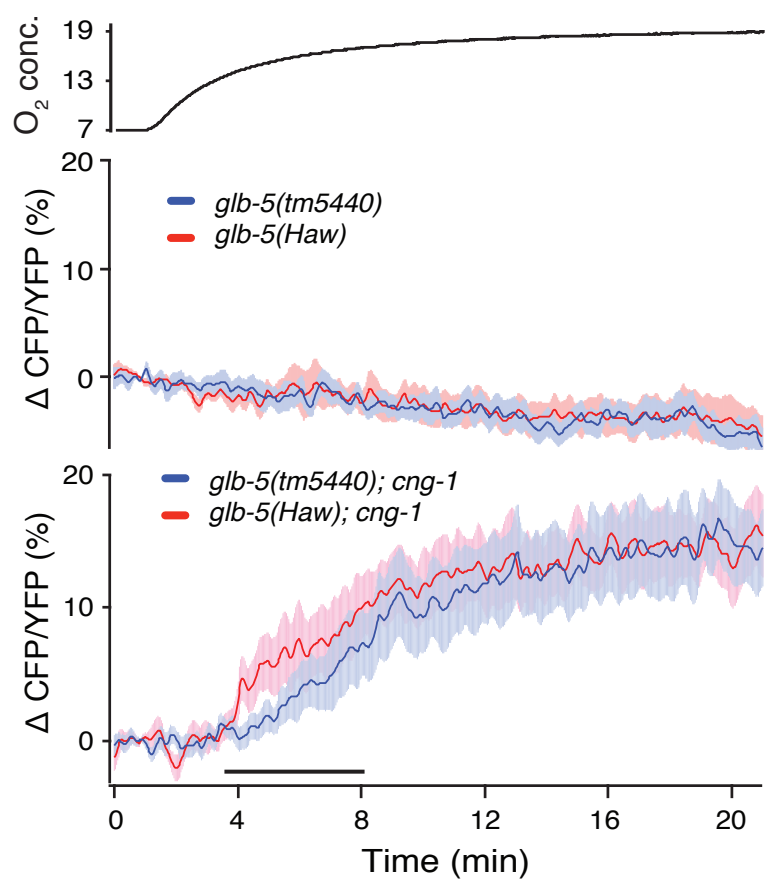


Supp Fig 4

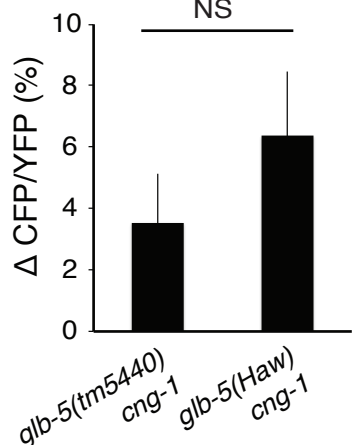
a



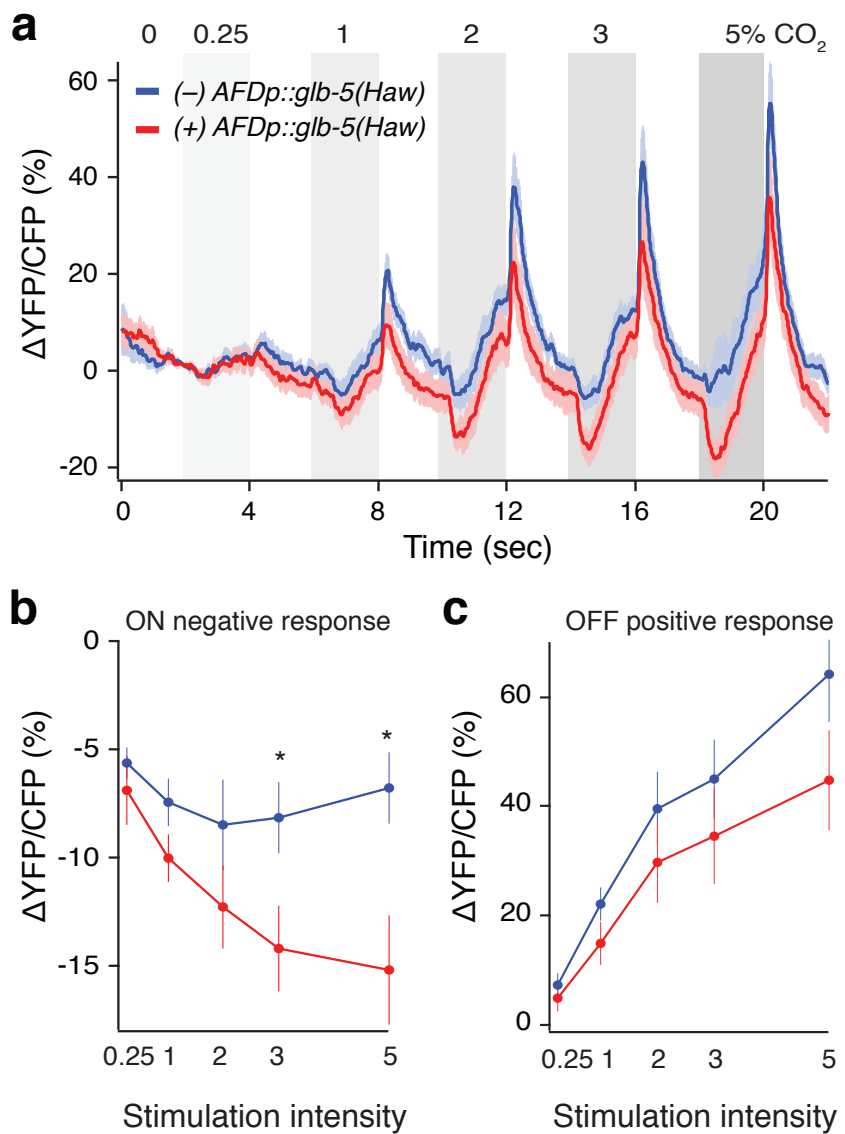
b



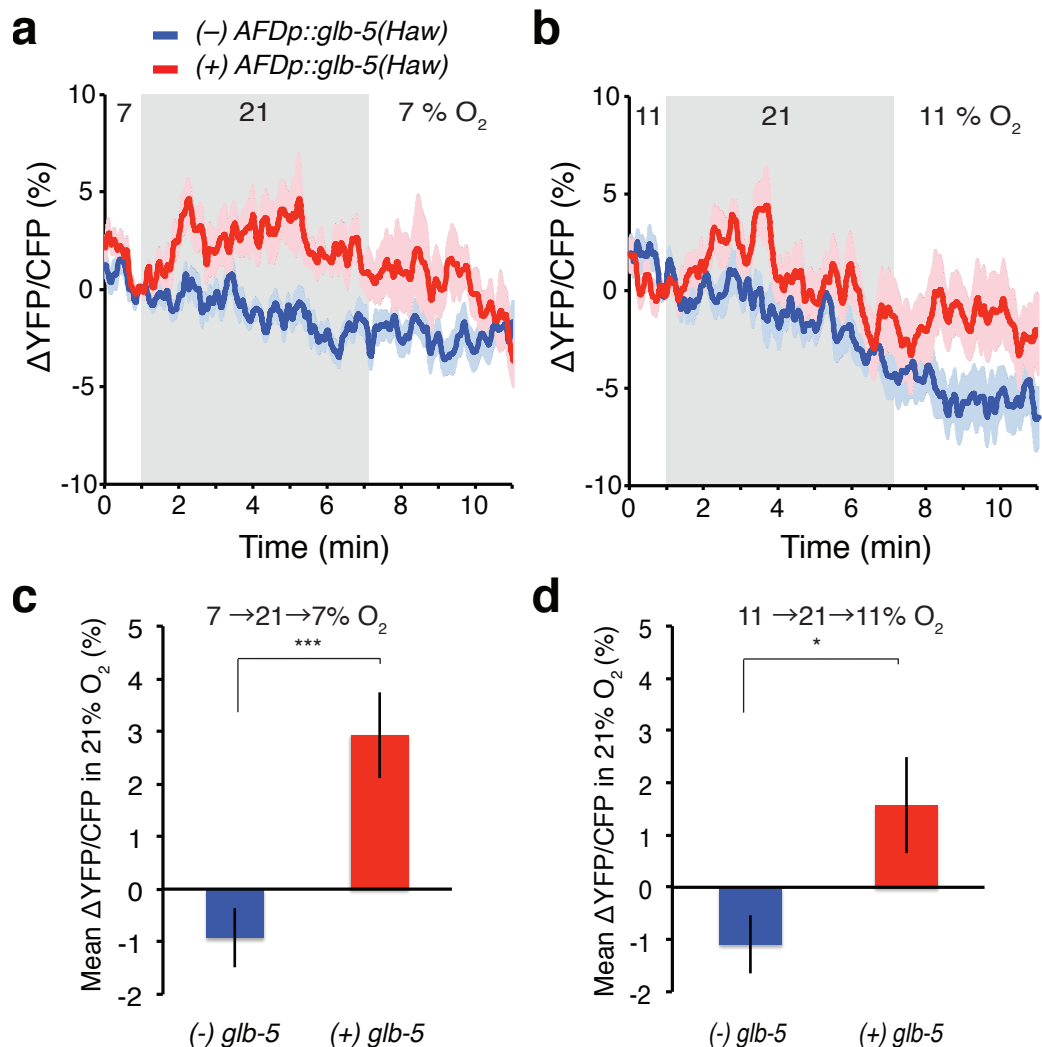
c



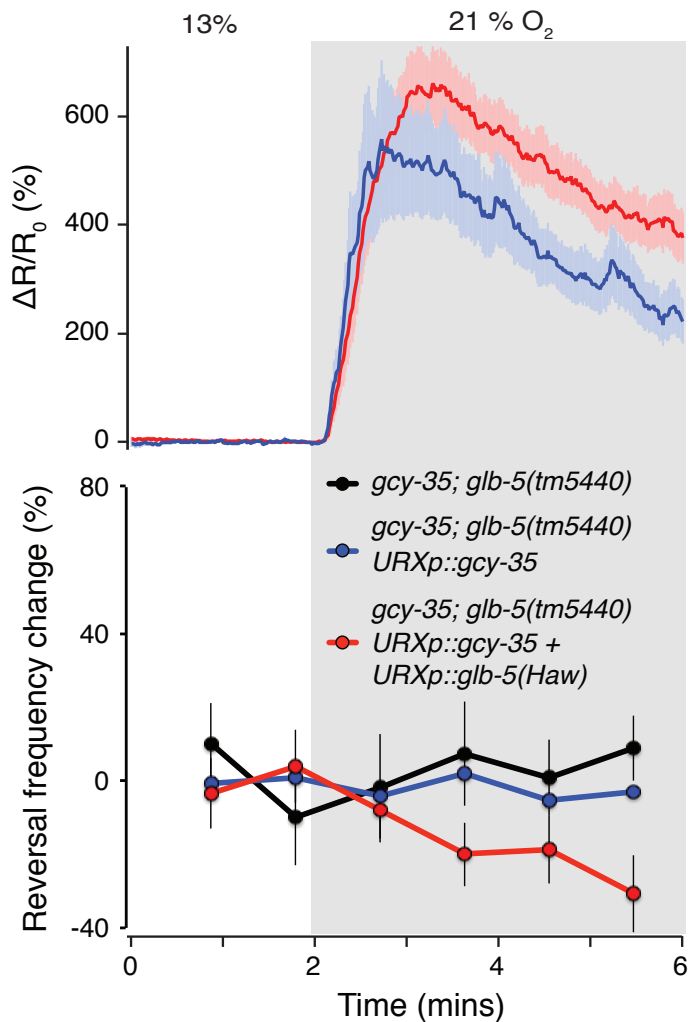
Supp Fig 5



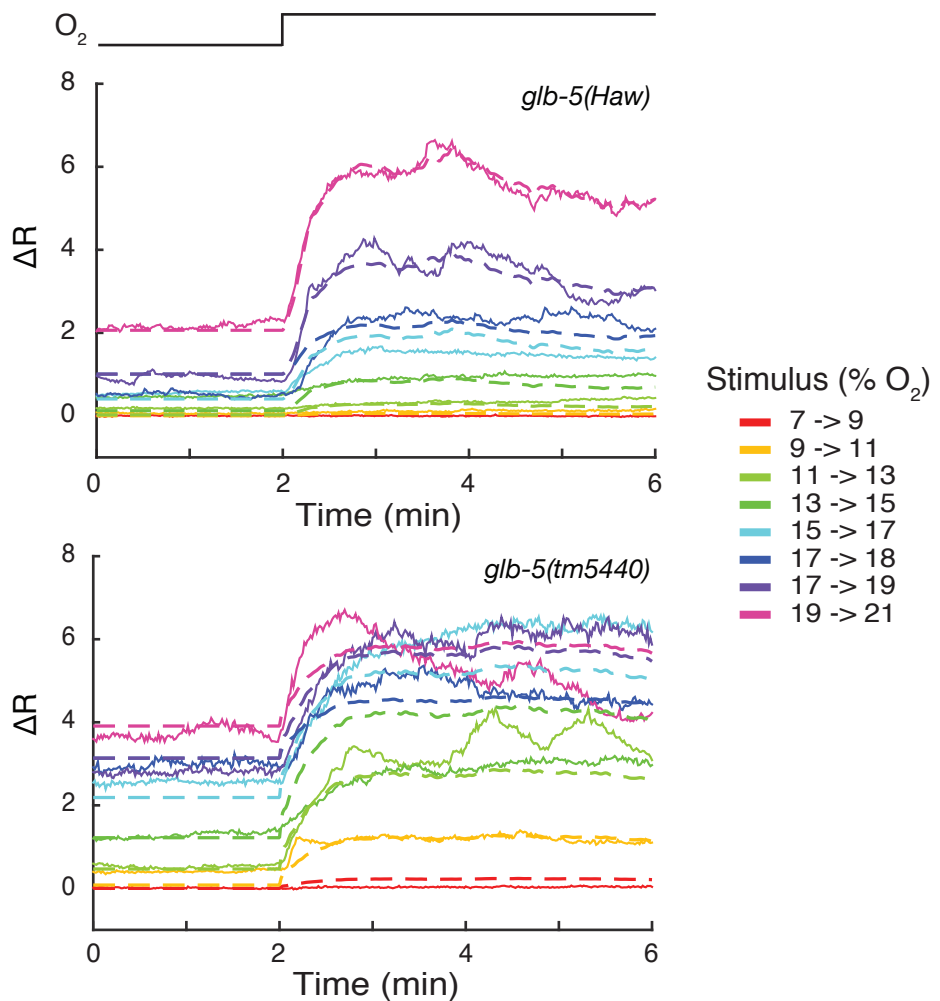
Supp Fig 6



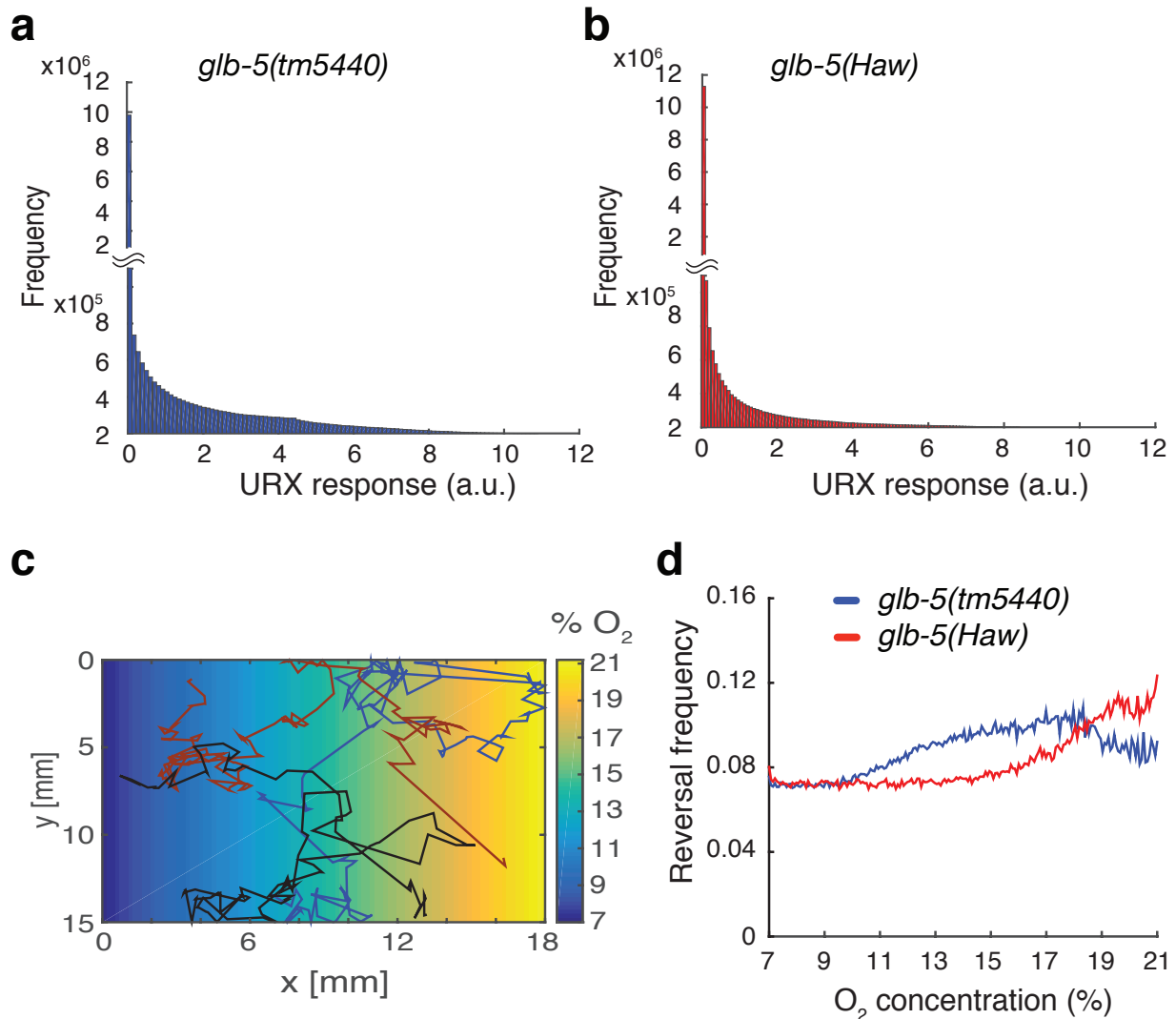
Supp Fig 7



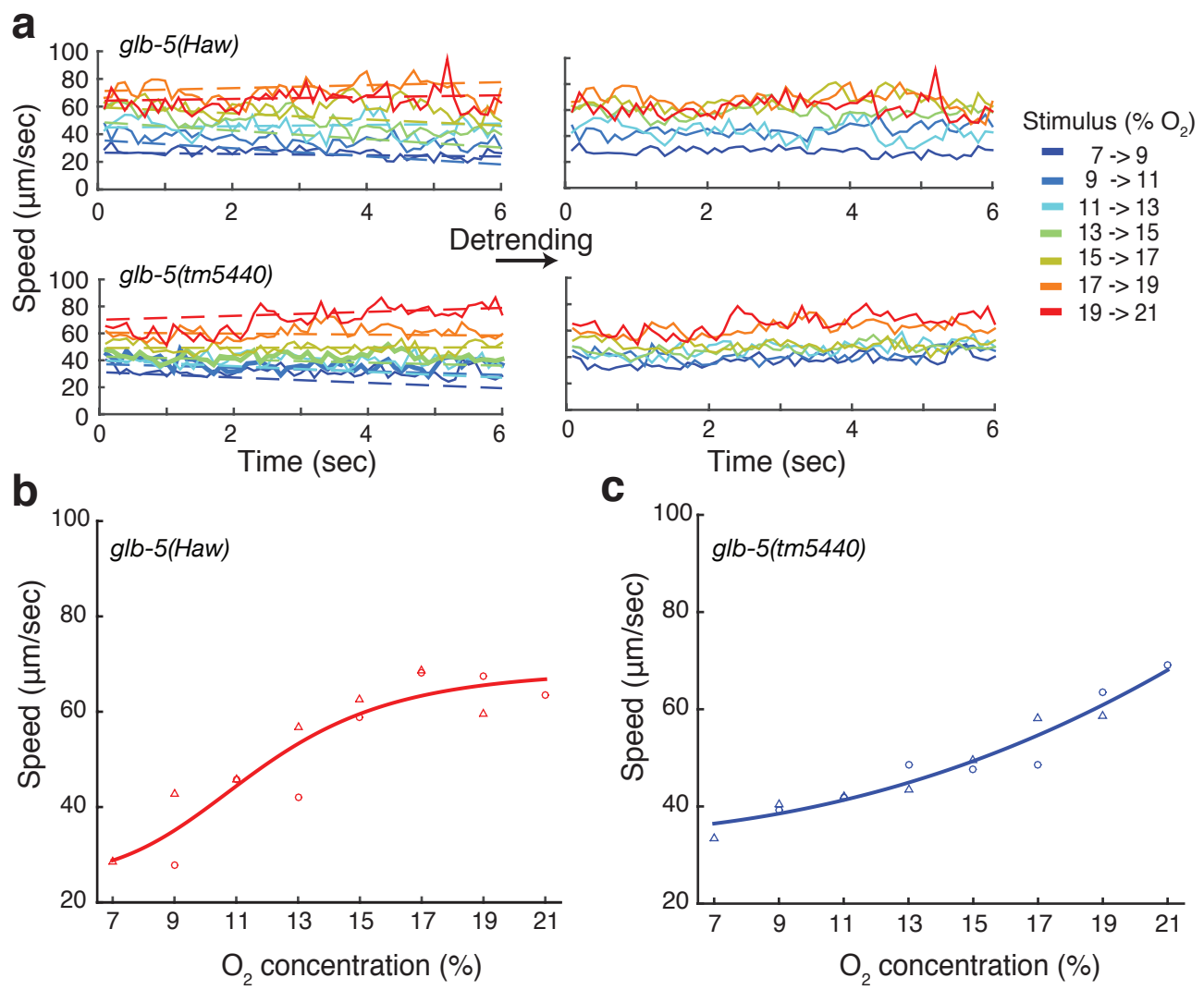
Supp Fig 8



Supp Fig 9



Supp Fig 10



Supp Fig 11

